iScience

CellPress
OPEN ACCESS

Article

ASC/inflammasome-independent pyroptosis in ovarian cancer cells through translational augmentation of caspase-1

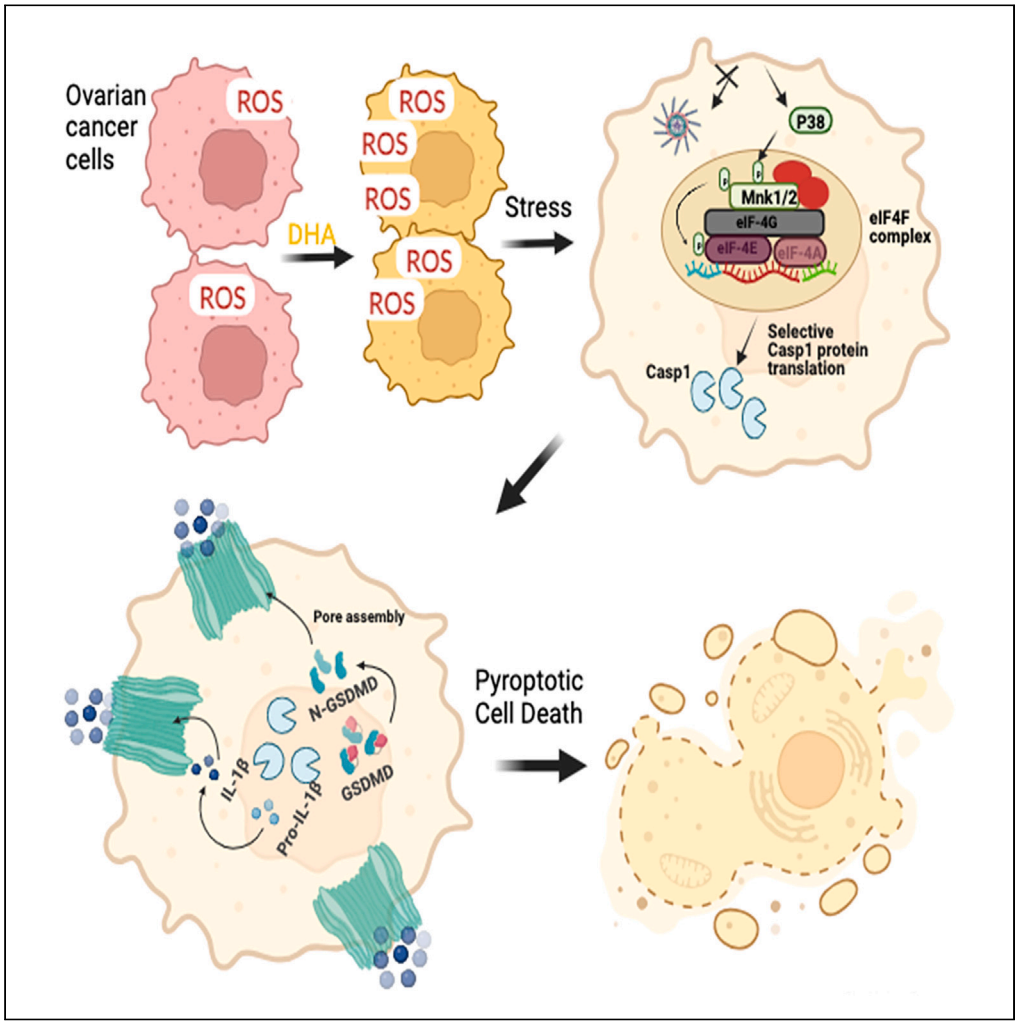

Ozlem Calbay, Ravi Padia, Mahmuda Akter, ..., Zheng Fu, Lingtao Jin, Shuang Huang

shuanghuang@ufl.edu

Highlights

Ovarian cancer cells can undergo pyroptosis independent of ASC/inflammasome

Ectopically overexpressing caspase-1 leads to caspase-1 activation and pyroptosis

DHA increases the abundance of caspase-1 at the level of protein translation

The $p38^{MAPK}$-Mnk1 signaling pathway mediates DHA-led caspase-1 protein synthesis

Calbay et al., iScience 26, 108408
December 15, 2023
https://doi.org/10.1016/j.isci.2023.108408

iScience

CellPress
OPEN ACCESS

Article

ASC/inflammasome-independent pyroptosis in ovarian cancer cells through translational augmentation of caspase-1

Ozlem Calbay,[1] Ravi Padia,[1] Mahmuda Akter,[1] Lei Sun,[1] Bin Li,[1] Nicole Qian,[1] Jianhui Guo,[1] Zheng Fu,[2] Lingtao Jin,[3] and Shuang Huang[1,4,*]

SUMMARY

Canonical pyroptosis is type of programmed cell death depending on active caspase-1, and the inflammasome carries out caspase-1 activation. Here, we showed that docosahexaenoic acid (DHA) induced ovarian cancer cell deaths in caspase-1-dependent manner. DHA increased caspase-1 activity and led to interleukin-1β secretion and gasdermin D cleavage while disulfiram inhibited DHA-induced cell death, suggesting that DHA triggered pyroptosis. Intriguingly, ASC, the molecule recruiting caspase-1 to inflammasome for activation, was dispensable for DHA-induced pyroptosis. Instead, we observed remarkable elevation in caspase-1 abundance concurrent with the activation of caspase-1 in DHA-treated cells. As ectopically overexpressing caspase-1 resulted in robust amount of active caspase-1, we reason that DHA activates caspase-1 and pyroptosis through the generation of excessive amount of caspase-1 protein. Mechanistically, DHA increased caspase-1 by specifically accelerating caspase-1 protein synthesis via the $p38^{MAPK}$/Mnk1 signaling pathway. We have uncovered an unknown pyroptosis mechanism in which caspase-1-dependent pyroptosis can occur without the participation of ASC/inflammasome.

INTRODUCTION

Pyroptosis is an inflammatory programmed cell death caused by microbial infection and executed by gasdermin family proteins. Upon the activation of caspase-1/4/5, active caspases generate the N-terminal of gasdermins which forms pores across the cell membrane, resulting in water influx and cell lysis accompanying the release of interleukin (IL) 1β and IL18.[1] Pyroptosis can be divided into canonical inflammasome and non-canonic inflammasome pathways, in which the former depends on caspase-1 activation whereas the latter is carried out by caspase-4/5.[2] Caspase-1, 4, and 5 are inactive monomer and require oligomerization to achieve catalytic competence. Caspase-1 activation is carried out by the multi-protein complexes termed inflammasome, which contain a sensor (NOD-like receptor, e.g., NLRP3 and NLRC4), a member of the HIN200/AIM2-like receptor family (AIM2), and a member of the TRIM family (Pyrin/TRIM20). Oligomerization of sensor proteins further recruits CARD domain-containing adaptor protein apoptosis associated speck like proteins (ASC). ASC brings in caspase-1 to inflammasomes for oligomerization, which leads to caspase-1 activation through the auto-cleavage.[3,4] Contrarily, oligomerizations of caspase-4 and 5 are inflammasome-independent and initiated by direct binding to intracellular lipopolysaccharide (LPS) via CARD domain.[5] Nevertheless, it is unknown whether caspase-1 activation can occur without the participation of inflammasome.

Mechanistic studies on pyroptosis are almost exclusively done in immune cells. Although pyroptosis can take place in non-immune cells, it is largely unknown whether it occurs in an identical or similar manner in immune cells. The presence of inflammasomes including NLRP3 has been reported in non-immune cells such as lung epithelial,[6] retinal pigment epithelial,[7] and colon cancer epithelial cells.[8] However, these early studies merely focused on the involvement of inflammasome in inflammatory responses and epithelial-mesenchymal transition while leaving its role in non-immune cell pyroptosis unaddressed. A recent study showed that forced expression of caspase-1 or caspase-11 p10/p20 activated domains was able to induce gasdermin D (GSDMD)-dependent pyroptosis in hepatocytes.[9] It remains unclear whether non-immune cells can respond to extracellular or intracellular stimuli to undergo pyroptosis in canonical or non-canonical inflammasome mechanisms.

Long chain omega-3 polyunsaturated fatty acids (PUFAs) including docosahexaenoic acid (DHA) and eicosapentaenoic acid (EPA) are being explored for their potential as anti-cancer agents because they possess potent anti-tumorigenic activities in diverse experimental models.[10] PUFAs can dose- and time-dependently induce cell death in a wide range of tumor cell types including colon,[11] pancreatic,[12]

[1]Department of Anatomy and Cell Biology, University of Florida College of Medicine, Gainesville, FL 32610, USA
[2]Department of Human and Molecular Genetics, VCU Institute of Molecular Medicine, VCU Massey Cancer Center, Virginia Commonwealth University, School of Medicine, Richmond, VA 23298, USA
[3]Department of Molecular Medicine, University of Texas Health San Antonio, San Antonio, TX 78229, USA
[4]Lead contact
*Correspondence: shuanghuang@ufl.edu
https://doi.org/10.1016/j.isci.2023.108408

breast,[13] and prostate cancer.[14] Almost all of these studies have suggested that apoptosis is the type of cell death induced by PUFA although the pathways leading to apoptosis vary from cell to cell. For example, EPA induced apoptosis in pancreatic cancer cells through reactive oxygen species (ROS) accumulation, caspase-8 activation, and autophagy induction[12] whereas DHA triggered prostate cancer cell apoptosis through syndecan-1 suppression of AKT signaling.[14] Interestingly, DHA was reported to induce pyroptosis in breast cancer MDA-MB-231 cells[15] and ferroptosis in fibrosarcoma HT1080 cells,[16] while pertinent mechanism was not clearly defined. Two recent studies suggest the therapeutic promise of DHA against ovarian cancer as it inhibited tumor growth and metastatic potential in preclinical ovarian cancer models.[17,18] Nevertheless, the exact mechanism underlying DHA suppression of ovarian cancer cell growth is elusive.

In this study, we demonstrate that DHA similarly suppressed ovarian cancer cell growth regardless whether the cells were epithelial or mesenchymal-like in nature. DHA acted by triggering pyroptosis in a caspase-1-dependent manner, as evidenced by caspase-1 activation, lactate dehydrogenase (LDH) release, IL1β secretion, and GSDMD cleavage. Surprisingly, ASC and NLRP3 were dispensable for DHA-induced pyroptosis, indicating that inflammasome is not involved in this DHA-induced event. Instead, we showed that DHA markedly increased the abundance of caspase-1 by accelerating caspase-1 protein synthesis. As exogenously overexpressing caspase-1 is sufficient to provoke caspase-1 activation and pyroptosis, we conclude that DHA induced ASC/inflammasome-independent pyroptosis in ovarian cancer cells through the translational augmentation of caspase-1. Finally, we revealed that the $p38^{MAPK}$/Mnk1 signaling pathway mediates DHA-led caspase-1 protein synthesis and subsequent pyroptosis in ovarian cancer cells.

RESULTS

DHA effectively induces ovarian cancer cell death

PUFA can induce cell death in diverse cell types, and apoptosis has been suggested as the responsive mechanism[19] although other cell death mechanisms have also been implicated.[15,16] To explore the effect of PUFA on the growth of ovarian cancer cells, varying concentrations of DHA, a PUFA containing 6 double bonds, were applied to a panel of established ovarian cancer cell lines for 3 days. MTT assay showed that DHA dose-dependently inhibited the growth of all of these cell lines (Figure 1A). To identify the cause of DHA-led growth inhibition, we performed propidium iodide (PI)-based flow cytometry to analyze cell cycle progression on ES2, SK-OV3, and OCC1 cells treated with vehicle or DHA for 24 and 48 h. While there was an only negligible sub-G1 population in vehicle-treated cells (control) at either time point, we detected a dramatic increase in sub-G1 population in cells treated with DHA at 24 h (Figure S1) and a much greater sub-G1 population at 48 h (Figure 1B), suggesting that DHA inhibits ovarian cancer cell growth by triggering cell death. Because the increase in the sub-G1 population (diminished DNA content) can be attributed to DNA damage/fragmentation, the hallmark of apoptosis, we further treated ES2 and SK-OV3 cells with DHA or apoptosis inducer staurosporine (STS) and paclitaxel. Western blot analysis showed that cleaved PARP and caspase-3 were readily seen in cells treated with STS or paclitaxel (Figures 1C and S2). Astonishingly, we failed to detect either PARP or caspase-3 cleavage in DHA-treated cells (Figures 1C and S2). In addition, we treated cells with DEVD, a caspase-3 inhibitor, prior to DHA treatment. MTT assay showed that DEVD exhibited a little protective effect on DHA-treated cells (Figure 1D). These results demonstrate that DHA is an effective ovarian cancer cell death inducer. Most notably, these results indicate that apoptosis is not the cell death mechanism responsible for DHA-induced ovarian cancer cell death.

DHA induces pyroptosis independent of ASC/inflammasome in ovarian cancer cells

In addition to apoptosis, diminished DNA content may also be observed in cells undergoing pyroptosis and necroptosis.[20,21] To characterize the mechanism underlying DHA-induced cell death, we treated ovarian cancer ES2, SK-OV3, and OCC1 cells with necrostatin (a necroptosis inhibitor) or YVAD (a caspase-1 inhibitor) followed by the addition of 100 μM DHA for 24 h. MTT assay showed that DHA-induced cell death was blocked by YVAD but not necrostatin (Figure 2A). Consistently, the microscopic examination also revealed that YVAD, but not necrostatin, prevented DHA from killing cells (Figure S3).

Pyroptosis is a programmed cell death mediated by caspase-1.[22] The observation that YVAD abrogated DHA-induced cell death prompted us to hypothesize that DHA triggered pyroptosis in ovarian cancer cells. To test this hypothesis, we measured caspase-1 activity in cells treated with vehicle or DHA and found that caspase-1 activity was approximately 100%, 65%, and 70% higher in DHA-treated ES2, SK-OV3, and OCC1 cells, respectively, than their vehicle-treated cells (Figure 2B). In subsequent experiments, we compared the level of released LDH activity in medium between vehicle and DHA-treated cells and found that DHA dose-dependently increased the amount of released LDH activity in all three tested cell lines (Figure 2C). Consistent with IL1β being a substrate of caspase-1, we detected substantial increase in IL-1β secretion in DHA-treated cells, as compared to the vehicle-treated control (Figure 2D). Also consistent with GSDMD as a caspase-1 substrate, we showed that DHA led to the reduction of pro-GSDMD and the appearance of cleaved GSDMD in ES2 and SK-OV3 cells (Figure 2E). To confirm the essence of cleaved GSDMD in DHA-induced cell death, cells were treated with DHA in the absence or presence of disulfiram, a GSDMD pore formation blocker.[23] MTT assay showed that disulfram lessened at least 50% of DHA-induced cell death (Figure 2F). Together, these results suggest that DHA induced ovarian cancer cell death through caspase-1-dependent pyroptosis.

In immune cells, caspase-1 is activated through ASC-facilitated oligomerization on the inflammasome.[22] To determine whether the same mechanism was responsible for DHA-induced caspase-1 activation and subsequent pyroptosis in ovarian cancer cells, we lentivirally introduced either scrambled sequence (control) or ASC short hairpin RNA (shRNA) into ES2, SK-OV3, and OCC1 cells to silence ASC1 (Figure S4). There was little alteration in DHA-induced cell death and LDH release between control and ASC-knockdown cells (Figures 3A and 3B). Moreover, MCC950, an inhibitor of NLRP3 (main inflammasome sensor participating caspase-1 activation), did not prevent DHA-induced cell death and LDH release (Figures 3C and 3D). During caspase-1-mediated pyroptosis, ASC has been reported to be present as a speck (oligomerized

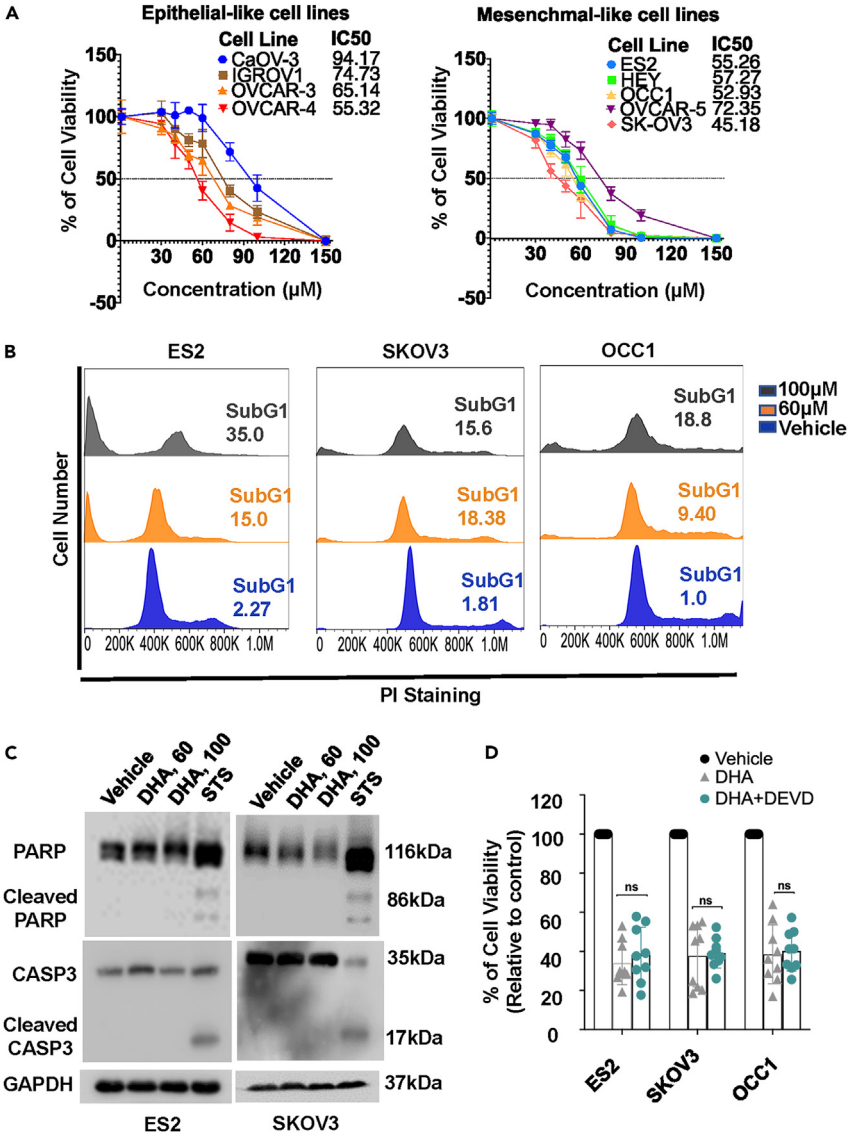

Figure 1. DHA induces ovarian cancer cell death in a non-apoptotic mechanism

(A) Overnight cultured cells were treated with varying concentration of DHA for 48 h, followed by an MTT assay to determine cell viability. Data are means ± SEM. n = 3.

(B) ES2, SK-OV3, and OCC1 cells were treated with vehicle, 60 or 100 μM DHA for 48 h, followed by PI-based flow cytometry to determine cell cycle progression.

(C) ES2 and SK-OV3 cells were treated with vehicle, 60, 100 μM DHA or 10 μM staurosporin (STS) for 24 h, followed by western blotting to detect PARP, cleaved caspase-3 (CASP3) and GAPDH with the respective antibodies.

(D) ES2, SK-OV3, and OCC1 cells were treated with vehicle or 100 μM DHA in the absence or presence of 10 μM DEVD for 24 h, followed by an MTT assay to analyze cell viability. % of cell viability was calculated as [(Control – Treatment)/Control] x 100. Control: vehicle-treated; Treatment: DHA or DHA + DEVD. Data are means ± SEM. ns, no significance.

ASC) in immune cells.[22] As would be expected, immunofluorescence staining with ASC monoclonal antibody (mAb) revealed ASC specks in murine macrophages stimulated with ATP (Figure 3E), a commonly used pyroptosis inducer in macrophages. However, we were unable to detect ASC speck in DHA-treated ovarian cancer cells (Figures 3F and S5). Taken together, these results suggest that, unlike pyroptosis in immune cells, ASC/inflammasome is not involved in DHA-induced pyroptosis in ovarian cancer cells.

DHA induces pyroptosis by increasing the abundance of caspase-1 in ovarian cancer cells

Previous studies demonstrate that non-canonical inflammasome caspase-4/5/11 activation ensues through the oligomerization bridged by LPS but not inflammasome.[2] We hypothesized that oligomization of caspase-1 and subsequent caspase-1 activation might have occurred

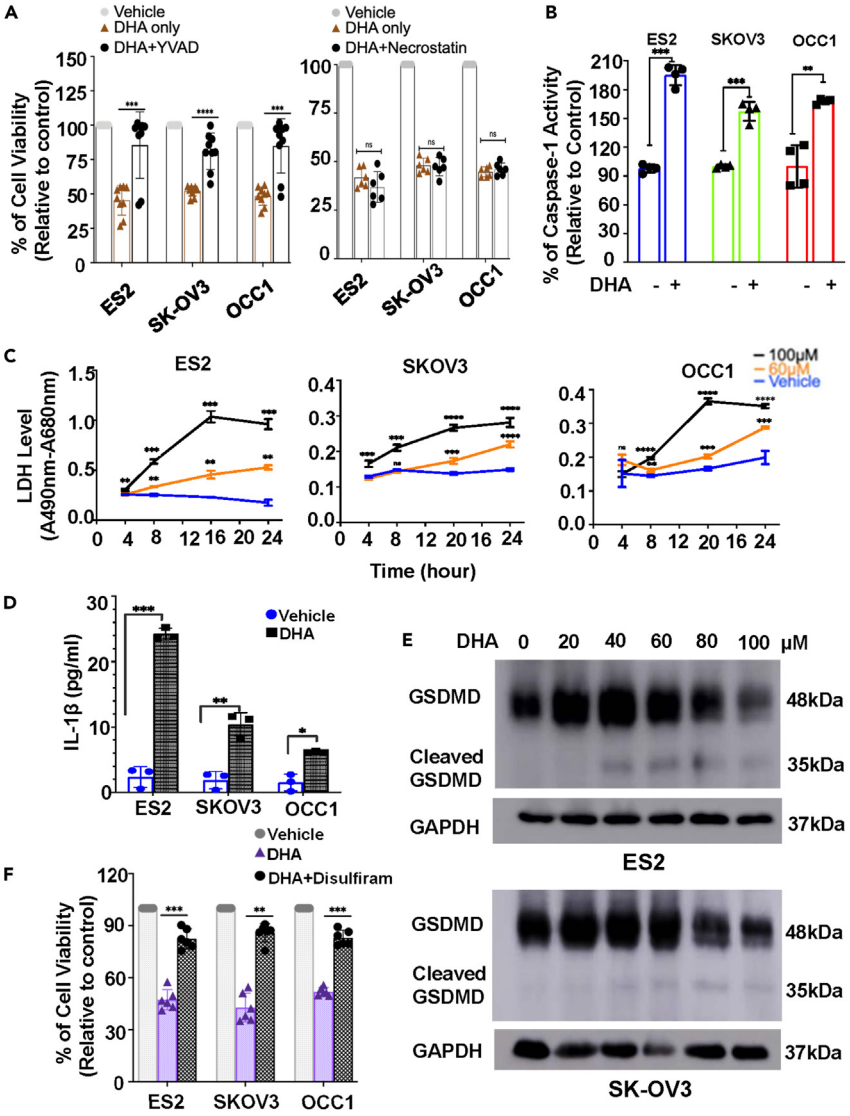

Figure 2. DHA induces pyroptosis in ovarian cancer cells

(A) ES2, SK-OV3, and OCC1 cells were treated with vehicle or 100 μM DHA in the absence or presence of 10 μM YVAD or 10 μM necrostatin for 24 h, followed by an MTT assay to analyze cell viability. % of cell viability was calculated as [(Control – Treatment)/Control] x 100. Control: vehicle-treated; Treatment: DHA, DHA + YVAD or DHA + necrostatin. Data are means ± SEM. ***, $p < 0.001$; ****, $p < 0.0001$; ns, no significance.

(B) ES2, SK-OV3, and OCC1 cells were treated with vehicle or 100 μM DHA for 24 h followed by analyzing caspase-1 activity. Control: vehicle. Data are means ± SEM. **, $p < 0.01$; ***, $p < 0.001$.

(C) ES2, SK-OV3, and OCC1 cells were treated with vehicle (Control) or 100 μM DHA for varying times and conditioned media were then collected to measure LDH activity. Data are means ± SEM. n = 3. **, $p < 0.01$, ***, $p < 0.001$; ****, $p < 0.0001$ vs. Control.

(D) ES2, SK-OV3, and OCC1 cells were treated with vehicle (Control) or 100 μM DHA for 24 h and conditioned media were then collected to measure the level of IL-1β. Data are means ± SEM. *, $p < 0.05$; **, $p < 0.01$, ***, $p < 0.001$.

(E) ES2 and SK-OV3 cells were treated with varying concentrations of DHA for 24 h, followed by western blotting to detect gasdermin D (GSDMD) and GAPDH with the respective antibodies.

(F) ES2, SK-OV3, and OCC1 cells were treated with vehicle or 100 μM DHA for 24 h in absence or presence of 10 μM disulfiram for 24 h, followed by an MTT assay to analyze cell viability. Data are means ± SEM. **, $p < 0.01$; ***, $p < 0.001$.

if there was an excessive amount of caspase-1. To test this hypothesis, we transfected varying amount of caspase-1-expressing plasmid into SK-OV3 cells. Western blot analysis showed that the level of caspase-1 gradually rose upon the increased amount of caspase-1-expressing plasmid and cleaved caspase-1 (active caspase-1) became visible with 0.3 μg plasmid (Figure 4A). Analysis of the conditioned media of caspase-1 plasmid-transfected SK-OV3 cells revealed a gradual rise in LDH release with the increased amount of plasmid (Figure 4B). These results support our hypothesis that excessive amount of caspase-1 can activate caspase-1 and induce pyroptosis.

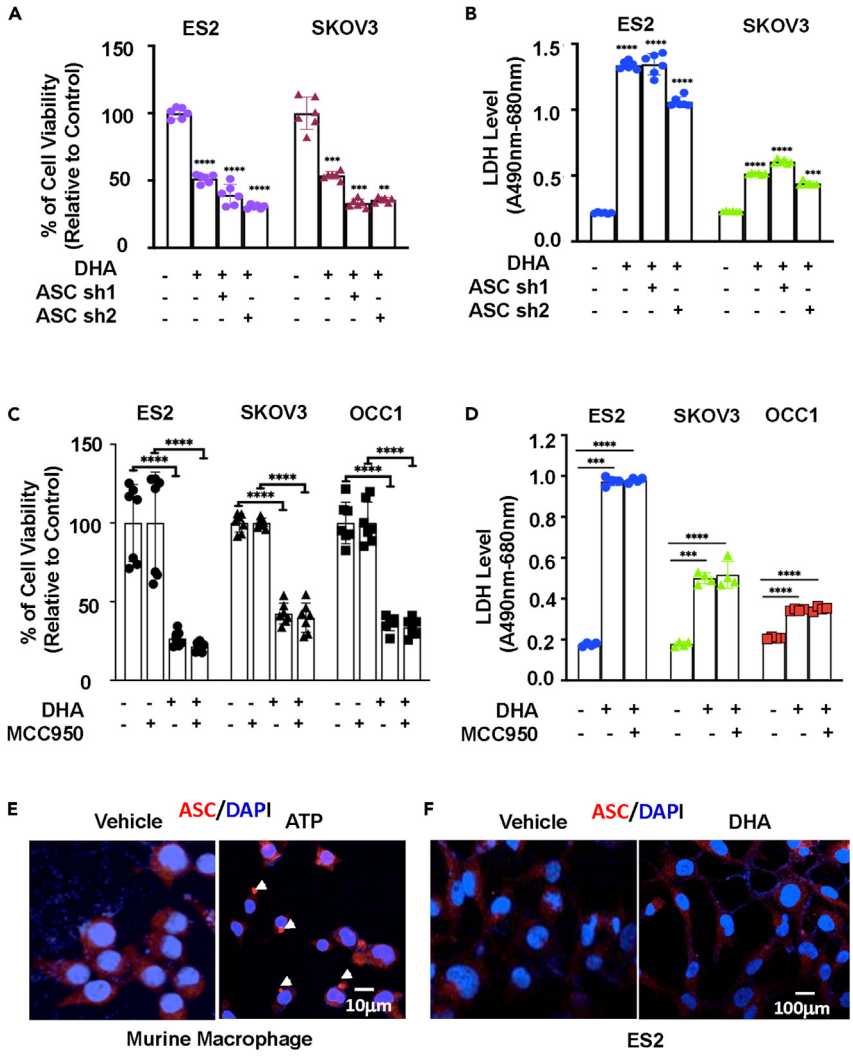

Figure 3. The inflammasome is not involved in DHA-induced pyroptosis

(A) To analyze cell viability, ES2 and SK-OV3 cells were lentivirally transduced with scramble or ASC shRNA for 3 days and then treated with vehicle or 100 μM DHA for 24 h, followed by an MTT assay. Data are means ± SEM. ****, $p < 0.0001$; ***, $p < 0.001$; **, $p < 0.01$.

(B) ES2 and SK-OV3 cells were lentivirally transduced with scramble or ASC shRNA for 3 days and then treated with vehicle or 100 μM DHA for 24 h. Conditioned media were collected to measure LDH activity. Data are means ± SEM. ****, $p < 0.0001$.

(C) ES2, SK-OV3, and OCC1 cells were treated with vehicle or 100 μM DHA in the absence or presence of 10 μM MCC950 for 24 h, followed by an MTT assay to analyze cell viability. Data are means ± SEM. ****, $p < 0.0001$.

(D) ES2, SK-OV3, and OCC1 cells were treated with vehicle or 100 μM DHA in the absence or presence of 10 μM MCC950 for 24 h, and conditioned media were collected to measure LDH activity. Data are means ± SEM. ***, $p < 0.001$; ****, $p < 0.0001$.

(E) Murine macrophages were treated with ATP for 1 h and then fixed for immunofluorescence staining with ASC antibody. DAPI was included for nuclear staining.

(F) ES2 cells were treated with 100 μM DHA for 24 h and then fixed for immunofluorescence staining with ASC antibody. DAPI was included for nuclear staining.

We next performed immunofluorescence staining to visualize caspase-1 in the vehicle and DHA-treated ES2, SK-OV3, and OCC1 cells. In vehicle-treated cells (control), caspase-1 staining was seen in the entire cytoplasm of these cells but the intensity was generally low (Figure 4C). Different from what was described in pyroptotic immune cells in which caspase-1 was present in the form of specks,[24,25] caspase-1 remained in a diffused pattern in the cytoplasm of DHA-treated cells (Figure 4C). However, we observed a remarkable increase in caspase-1 staining in DHA-treated cells in comparison to controls (Figure 4C). In parallel, we treated cells with varying concentration of DHA for 24 h followed by western blot analysis to detect caspase-1. DHA dose-dependently elevated the level of caspase-1 in all cell lines, and cleaved caspase-1 emerged in samples displaying marked caspase-1 induction (Figure 4D). To generalize our findings, we also treated OVCAR3 and OVCAR4 cells, two well-characterized high-grade serous ovarian cancer (HGSOC) lines, with DHA. Similarly, DHA dose-dependently upregulated the level of caspase-1 and cleaved caspase-1 was again detected in sample with significant induction of caspase-1 (Figure S6).

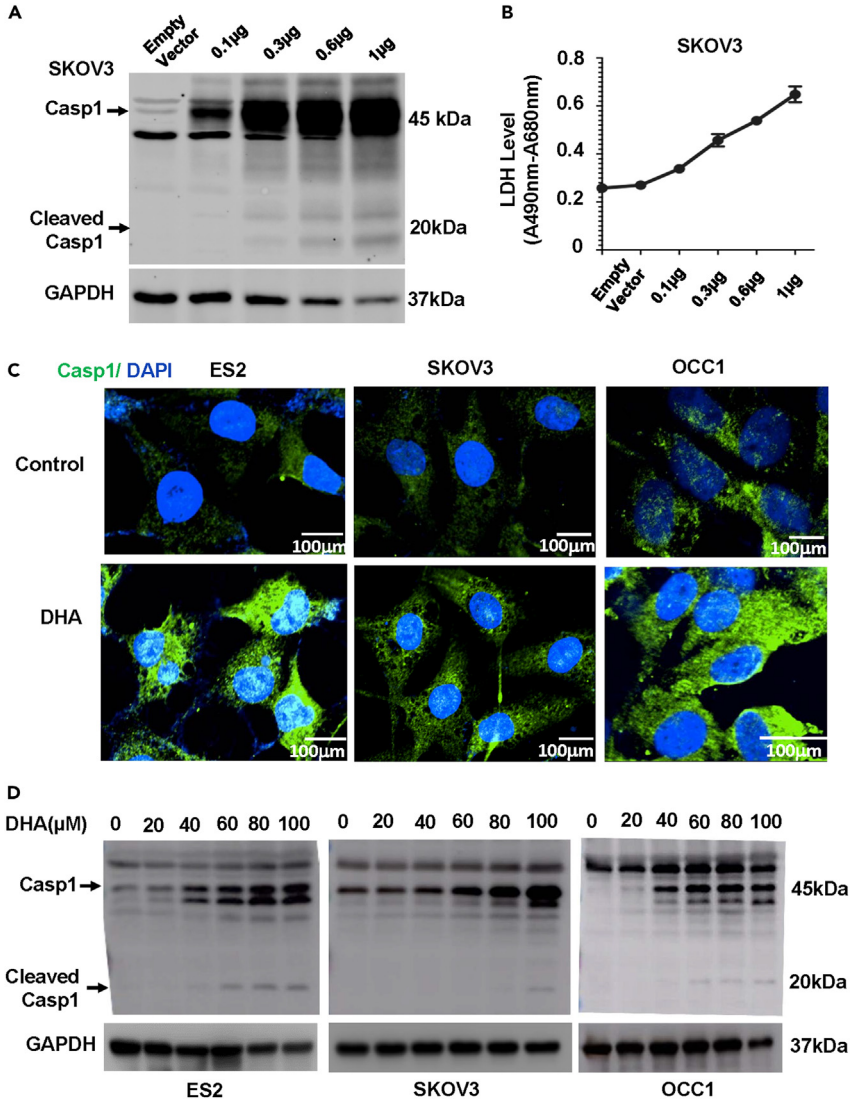

Figure 4. Augmentation of caspase-1 is sufficient for caspase-1 activation

(A) SK-OV3 cells were transfected with varying amount of plasmid encoding caspase-1 for 24 h and then lysed for western blotting to detect caspase-1 (Casp1) and GAPDH with the respective antibodies.

(B) SK-OV3 cells were transfected with varying amount of plasmid encoding caspase-1 for 24 h and conditioned media were then collected to measure LDH activity. Data are means ± SEM. n = 3.

(C) ES2, SK-OV3 and OCC1 cells were treated with vehicle (Control) or 100μM DHA and then fixed for immunofluorescence staining with caspase-1 antibody. DAPI was included for nuclear staining.

(D) ES2, SK-OV3, and OCC1 cells were treated with varying concentration of DHA for 24 h followed by western blotting to detect caspase-1 and GAPDH with the respective antibodies.

Collectively, these results implicate that DHA triggers pyroptosis in ovarian cancer cells by inducing an excess amount of caspase-1 rather than through ASC-facilitated caspase-1 oligomerization.

Recent studies showed that DHA was able to inhibit tumor growth in preclinical ovarian cancer models.[17,18] To link anti-tumorigenic effect of DHA to pyroptosis, female athymic nude mice were intraperitoneally injected with luciferase-expressing ES2 cells. One week after ES2 cell injection, mice were intraperitoneally administrated with DHA or vehicle once a day. Weekly bioluminescence imaging showed rapid peritoneal xenograft development in mice receiving only vehicle (Figures 5A and 5B). In contrast, administrating DHA hindered this process (Figures 5A and 5B). At the end of treatment, all mice were euthanized and tumor implants were collected. Average weight of tumor implant was significantly less in DHA-treated mice than that in vehicle-treated ones (Figure 5C). Further immunohistochemistry staining showed little caspase-1 but strong Ki67 staining in tumors excised from vehicle-treated mice (Figure 5D). In contrast, tumors derived from DHA-treated

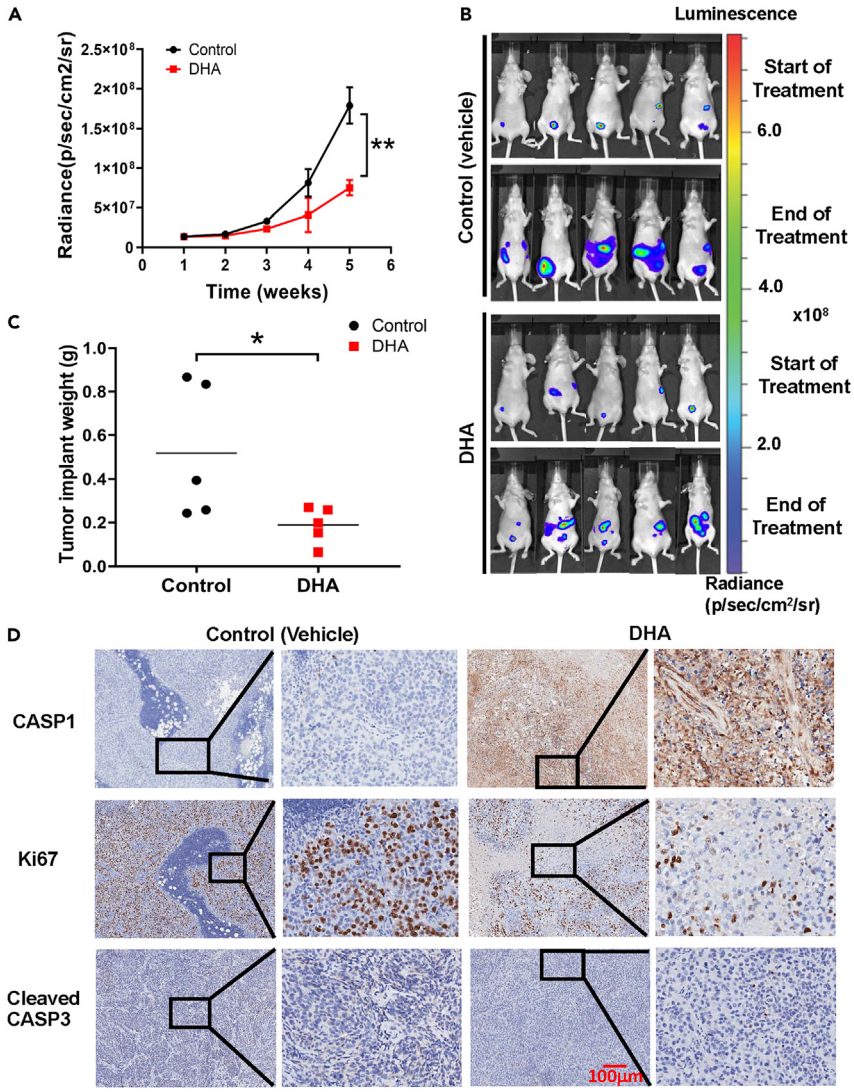

Figure 5. DHA suppresses peritoneal xenograft development

(*A*) Luciferase-expressing ES2 cells (10^6 cells/mouse) were intraperitoneally injected into female athymic nude mice. One week after tumor cell injection, mice were divided into two groups: one was treated with vehicle (DMSO) (control) and the other with DHA (15 mg/kg). Xenograft development was monitored weekly using the Xenogen IVIS-200 *In Vivo* bioluminescence imaging system. Data are means ± SD. n = 5. **, $p < 0.01$.

(*B*) Bioluminescent images of the xenograft tumors at the start (week 1) and end of treatment (week 5). The image data are displayed in radiance (photons/sec/cm2/steradian).

(*C*) Mice were sacrificed after 4 weeks of treatment and tumor implants for weight measurement. Data are means ± SD. *, $p < 0.05$.

(*D*) Representative pictures of IHC staining on caspase-1 (CASP1), cleaved caspase-3 (cleaved CASP3), and Ki67 in tumor tissues.

mice displayed robust caspase-1 but greatly reduced Ki67 staining (Figure 5D). In addition, we were unable to detect cleaved caspase-3 staining in tumors derived from either vehicle or DHA-treated mice (Figure 5D). These results provide further evidence that DHA deters xenograft development by inducing pytoptosis through elevating caspase-1 expression rather than triggering apoptosis.

DHA upsurges the abundance of caspase-1 at the level of protein synthesis

To elucidate the molecular mechanism underlying DHA-led elevation of caspase-1 protein, we treated ES2 and OCC1 cells with DHA at their respective half maximal inhibitory concentration (IC_{50}) for various times followed by western blotting and RT-qPCR to assess the levels of caspase-1 protein and mRNA, respectively. While DHA increased the level of caspase-1 protein from as early as 4 h in both cell lines (Figure 6A), there was little change in the level of caspase-1 mRNA (Figure 6B), indicating that DHA enhances the amount of caspase-1 protein on the level of protein. As the abundance of protein reflects the dynamic change between the rates of protein synthesis and protein

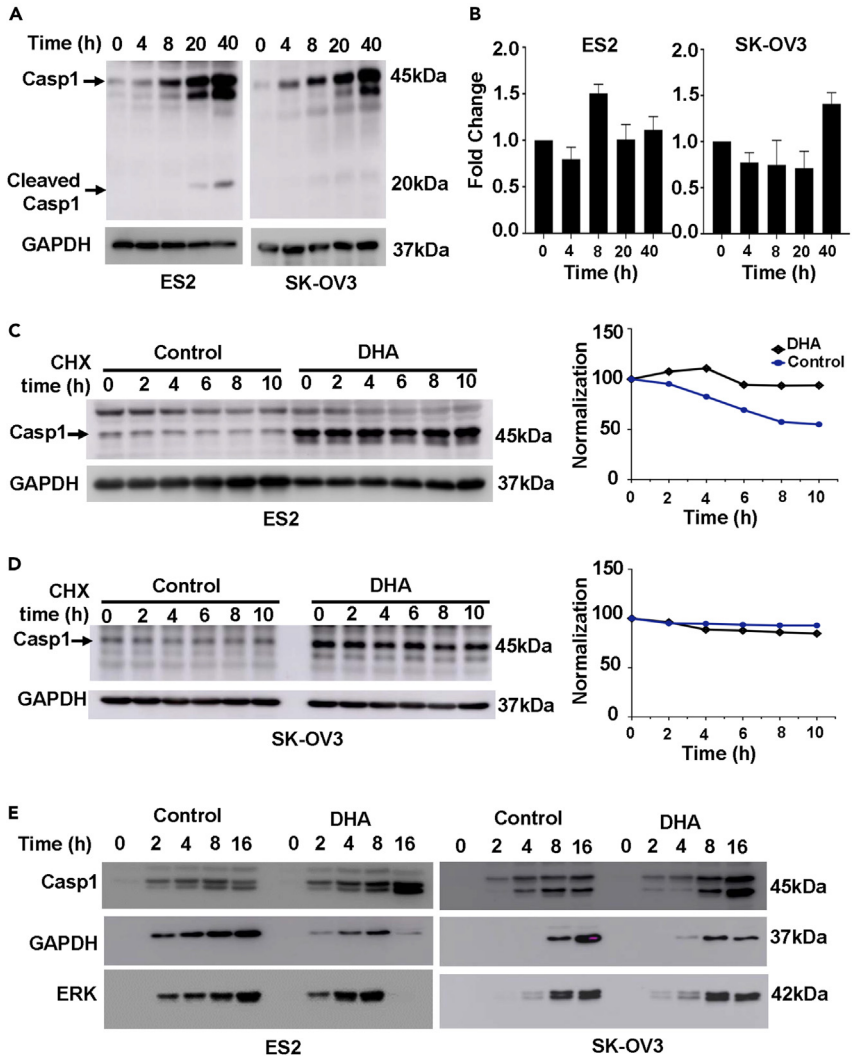

Figure 6. DHA enhances caspase-1 abundance by accelerating caspase-1 protein synthesis

(A) ES2 and OCC1 cells were treated with DHA at IC_{50} for varying times followed by western blotting to detect caspase-1 and GAPDH with the respective antibodies.

(B) ES2 and OCC1 cells were treated with DHA at IC50 for varying times followed by RT-qPCR to measure the level of caspase-1 mRNA. β-Actin mRNA was used as an internal control for standardization. Data are means ± SEM.

(C and D) ES2 (C) and OCC1 (D) cells were treated with DHA at IC50 for 16 h, followed by the addition of 10 μg/ml cycloheximide. At varying times, cells were harvested for western blotting to detect caspase-1 and GAPDH with the respective antibodies. Intensities of both caspase-1 and GAPDH bands were quantitated using a densitometer. The intensity of the caspase-1 band at each time point was normalized by the intensity of GAPDH at the corresponding time point.

(E) ES2 and OCC1 cells were cultured in a methione-free medium for 2 h, and then fed with a medium containing AHA. At varying times, cells were lysed and AHA-incorporated proteins were isolated for western blotting to detect caspase-1, GAPDH, and ERK with the respective antibodies.

degradation,[26] we first examined caspase-1 protein stability by cycloheximide chasing assay. Western blot with cell lysates collected from ES2 or OCC1 cells treated with vehicle (control) or IC_{50} of DHA for varying times showed that DHA moderately prolonged the half-life of caspase-1 protein in ES2 (Figure 6C) but did not affect caspase-1 protein stability in OCC1 cells (Figure 6D). We next assayed caspase-1 protein synthesis rate in the vehicle and DHA-treated cells by feeding methionine-starved cells with L-Azidohomoalanine (AHA), a methionine analog, for varying times. Because all newly synthesized proteins contain AHA, the protein synthesis rate is thus proportional to the amount of AHA-containing proteins.[27] By analyzing the amount of AHA-containing caspase-1, we found that caspase-1 protein synthesis was much faster in DHA-treated cells than in vehicle-treated ones (control) (Figure 6E). Nevertheless, the protein synthesis rate of GAPDH and ERK was slower in DHA-treated cells than that in control (Figure 6E). These results suggest that increased caspase-1 protein synthesis is the principal factor for DHA-led caspase-1 protein elevation and subsequent pyroptosis in ovarian cancer cells. Moreover, selective acceleration of caspase-1 protein synthesis, but suppression of protein synthesis of GAPDH and ERK2 in DHA-treated cells, also indicates that DHA-led upsurge of

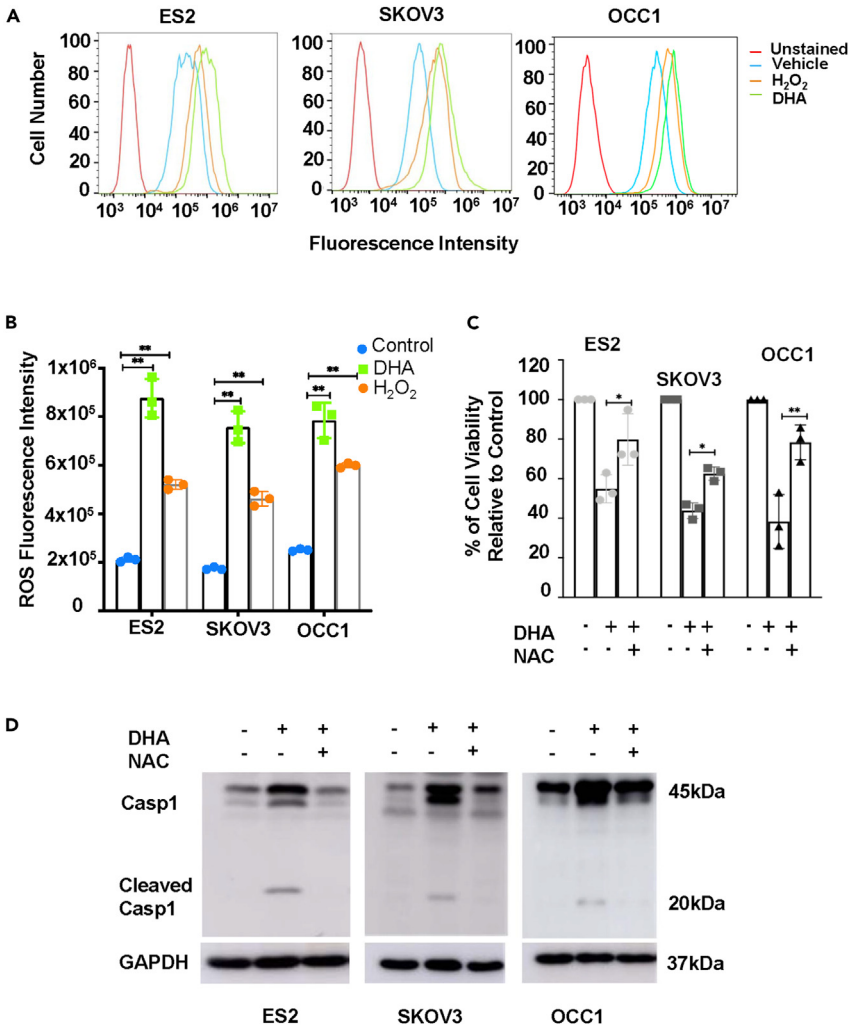

Figure 7. ROS is a mediator of DHA-induced surge in caspase-1 abundance

(A and B) ES2, SK-OV3, and OCC1 cells were treated with vehicle (Control), 100 μM DHA or H2O2 followed by flow cytometry to measure ROS fluorescence intensity (A, flow cytometry; B, quantitation).

(C) ES2, SK-OV3, and OCC1 cells were treated with vehicle or 100 μM DHA in the absence or presence of 5mM NAC for 24 h, followed by an MTT assay to analyze cell viability. % of cell viability was calculated as [(Control – Treatment)/Control] x 100. Control: vehicle-treated; Treatment: DHA or DHA + NAC. Data are means ± SEM. *, $p < 0.05$; **, $p < 0.001$.

(D) ES2, SK-OV3, and OCC1 cells were treated with 100 μM DHA in the absence or presence of 5mM NAC for 24 h followed by western blotting to detect caspase-1 and GAPDH with the respective antibodies.

caspase-1 protein is likely to be mediated by cellular stress as cellular stresses including ROS often lead to diminished global protein synthesis.[28]

DHA-led ROS accumulation is critical for an increased level of caspase-1 protein

Early studies have demonstrated that DHA possesses the ability to boost cellular ROS in diverse cell types.[29,30] This raised the possibility that DHA accelerated caspase-1 protein synthesis through the increase of cellular ROS in ovarian cancer cells. To test this possibility, we treated ES2, SK-OV3, and OCC1 cells with the vehicle, H_2O_2, or DHA followed by DCFDA/H2DCFDA-based flow cytometry. As would be expected, H_2O_2 elevated the level of ROS in comparison to vehicle control (Figure 7A). In all three cell lines, DHA increased the levels of ROS even more than H_2O_2 (Figures 7A and 7B; results of time course are in Figures S7A and S7B). To investigate whether ROS is required for DHA-induced cell death, we pretreated cells with N-acetyl-L-cysteine (NAC), an antioxidant, prior to DHA treatment. MTT assay showed that NAC impaired the ability of DHA to reduce cell viability (Figure 7C). Moreover, NAC largely blocked DHA-induced caspase-1 upregulation and activation in all tested cell lines (Figure 7D). These results suggest that ROS is at least one of the mediators of DHA for increasing caspase-1 protein abundance and subsequent pyroptosis in ovarian cancer cells.

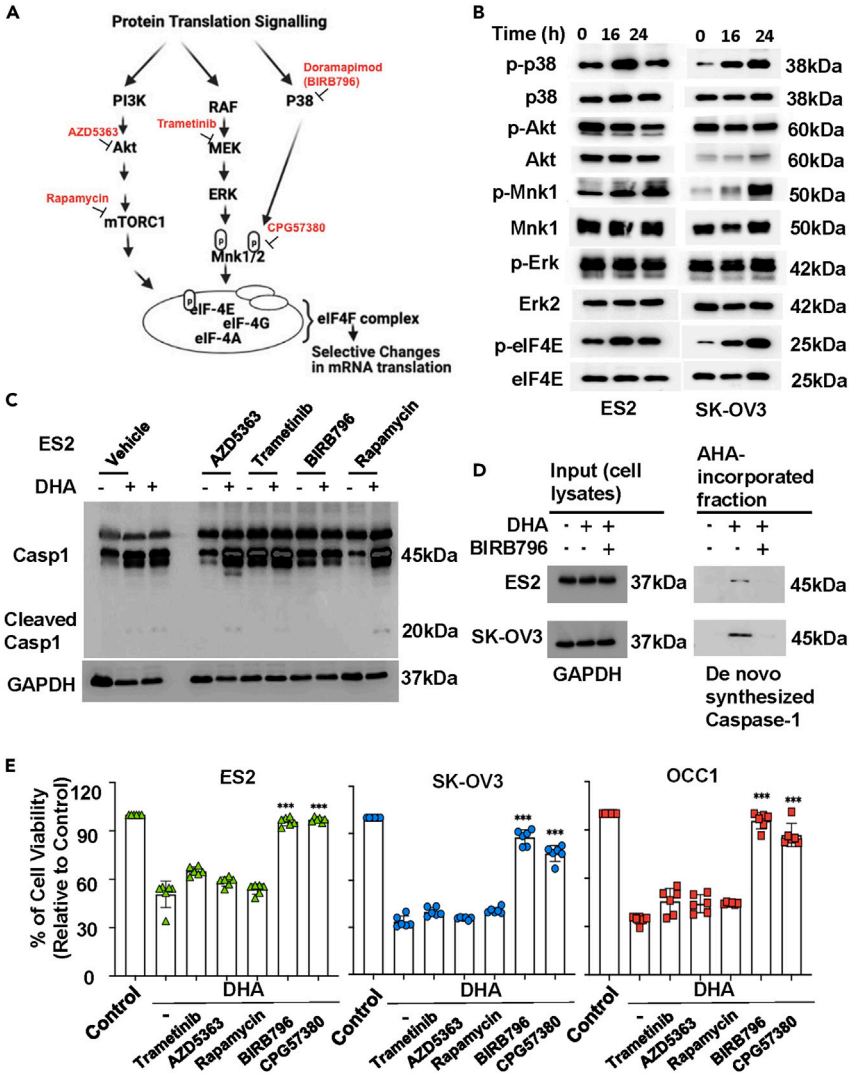

Figure 8. DHA accelerates caspase-1 protein synthesis in a p38MAP-dependent manner

(A) Protein synthesis signaling diagram. Inhibitors for signaling components are denoted in red.

(B) ES2 and SK-OV3 cells were treated with DHA at IC50 for 16 or 24 h, followed by western blotting to detect phosphor-p38MAPK, p38MAPK, phosphor-Akt, Akt, phosphor-Mnk1, Mnk1, phosphor-Erk, Erk, phosphor-eIF4E, and eIF4E with the respective antibodies.

(C) ES2 cells were treated with DHA in the absence or presence of AZD5383, Trametinib, BIRB796, or Rapamycin for 24 h, followed by western blotting to detect caspase-1 and GAPDH with the respective antibodies.

(D) ES2 and SK-OV3 cells were cultured in a methionine-free medium for 2 h, and then fed with a medium containing AHA in the absence or presence of BIRB796 for 16 h. Cells were lysed and AHA-incorporated proteins were isolated for western blotting to detect caspase-1 with caspase-1 antibody. Cell lysates before isolating AHA-incorporated proteins were also subjected to western blotting to detect GAPDH to ensure equal loading.

(E) ES2, SK-OV3, and OCC1 cells were treated with vehicle or 100 μM DHA in the absence or presence of AZD5363, Trametinib, Rapamycin, BIRB796, or 796 CPG57380 for 24 h followed by MTT assay to analyze cell viability. % of cell viability was calculated as [(Control – Treatment)/Control] x 100. Control: vehicle-treated; Treatment: DHA or DHA + inhibitors. Data are means ± SEM. ***, $p < 0.001$.

p38^{MAPK} signaling participates in DHA-induced caspase-1 protein translation and pyroptosis

Three signaling pathways that control protein translation (synthesis) are PI3K/Akt/mTOR, MEK/Erk/Mnk1, and p38^{MAPK}/Mnk1 (Figure 8A).[31] To identify the pertinent signaling pathway critical for DHA-induced caspase-1 protein synthesis, we treated ES2 and SK-OV3 cells with IC_{50} of DHA for 16 and 24 h followed by western blotting to assess the activation of these pathways. DHA increased the levels of phosphor-p38^{MAPK}, phosphor-Mnk1, and phosphor-eIF4E but not phosphor-Akt nor phosphor-Erk (Figure 8B), indicating that the p38^{MAPK}/Mnk1 signaling pathway is specifically involved in DHA-induced caspase-1 synthesis. In a parallel experiment, we pretreated ES2 cells with specific inhibitors to p38^{MAPK} (BIRB796), MEK (Trametinib), Akt (AZD5363), or mTORC1 (rapamycin) followed by DHA

treatment. Western blot analysis showed that $p38^{MAPK}$ inhibitor BIRB796 blocked DHA-induced caspase-1 upregulation whereas inhibitors to Akt and mTROC1 were unable to interfere with DHA-led caspase-1 surge (Figure 8C). MEK inhibitor (Trametinib) alone increased the level of caspase-1 but did not appear to disable DHA to enhance caspase-1 abundance (Figure 8C). In addition, AHA-based *de novo* protein synthesis assay showed that $p38^{MAPK}$ inhibitor BIRB786 abrogated DHA-induced caspase-1 synthesis in both ES2 and SK-OV3 cells (Figure 8D). These results suggest that the $p38^{MAPK}$ signaling pathway mediates DHA-induced caspase-1 protein synthesis in ovarian cancer cells.

To link $p38^{MAPK}$ regulation of DHA-induced caspase-1 protein synthesis to pyroptosis, we treated ES2, SK-OV3, and OCC1 cells with DHA in the absence or presence of rapamycin, trametinib, BIRB796, or CPG57380 for 24 h followed by crystal violet staining to evaluate cell viability. BIR8796 and CPG57380 abolished DHA-induced cell death whereas other inhibitors were ineffective (Figure 8E). Consistently, BIR8796 and CPG57380 blocked DHA-induced IL-1β secretion and LDH release (Figures S8A and S8B). These results suggest that DHA, through the induction of ROS and the activation of the $p38^{MAP}$/Mnk1 signaling pathway, accelerates caspase-1 protein synthesis, which in turn results in pyroptosis in ovarian cancer cells.

DISCUSSION

PUFAs, including DHA, induce cell death through a mechanism of apoptosis in a wide spectrum of cancer cell types.[10] Intriguingly, this study showed that DHA killed ovarian cancer cells through caspase-1-mediated pyrotosis but not apoptosis. Different from canonic inflammasome pyroptosis, ASC/NLRP3 inflammasome was not involved in DHA-led caspase-1 activation. Instead, we found that DHA markedly increased abundance of caspase-1 protein. Since forced expression of caspase-1 was sufficient to induce pyroptosis, we conclude that DHA induces pyroptosis by massively increasing the amount of caspase-1 protein. Mechanistically, we showed that DHA amassed caspase-1 protein by accelerating caspase-1 protein synthesis via the $p38^{MAPK}$/Mnk1 signaling pathway.

In immune cells, caspase-1 activation is accomplished through ASC-mediated pro-caspase-1 recruitment to the inflammasome and the subsequent oligomerization.[3] Targeting various inflammasome subunits including ASC and NLRP3 through inhibitors or depletion can effectively abolish pyroptosis.[32,33] Our initial hypothesis was that DHA initiated ovarian cancer cell pyroptosis in a similar manner. Quite in the contrary, we found that depletion of ASC or inhibiting NLRP3 with MCC950 exhibited little effect on DHA-induced caspase-1 activation and cell death, indicating that DHA-led caspase-1 activation and pyroptosis occur in a mechanism not involving in ASC or NLRP3. Two recent studies reported that DHA inhibits inflammasome activation in immune cells,[34,35] which actually argue the participating of inflammasome in DHA-led caspase-1 activation.

An early study showed that anthrax lethal toxin (LeTx) was able to activate caspase-1 through NLRP1b inflammasome in ASC-null macrophages.[36] However, NLRP1b inflammasome apparently only served as an alternative mechanism because LeTx induced ASC speck and activated caspase-1 in an ASC-dependent manner in wild-type macrophages. In contrast, DHA failed to induce ASC speck but strongly activated caspase-1 even ASC was readily detected in ovarian cancer cells. Such stark difference indicates that DHA is unlikely to act through NLRP1b. To elucidate molecular mechanism underlying DHA-led caspase-1 activation, we found that DHA massively accumulated caspase-1 protein in ovarian cancer cells and active caspase-1 could be detected in samples with greatly elevated level of caspase-1. Since the oligomerization of caspase-1 is a necessity for caspase-1 activation,[4] we envisaged that overproduction of caspase-1 might be sufficient for caspase-1 oligomerization and subsequent caspase-1 activation. To support this possibility, we showed that transfection of expression plasmid encoding caspase-1 resulted in caspase-1 activation and pyroptosis. Our results are consistent with an early report in which forced expression of caspase-1 induced GSDMD-dependent pyroptosis in hepatocytes although this study did not examine the potential involvement of inflammasome.[9] Taken together, we reason that DHA-led caspase-1 activation results from greatly upregulated caspase-1 abundance. To our knowledge, our study is the first one demonstrating that caspase-1 activation and caspase-1-mediated pyroptosis can occur independent of ASC/inflammasome in cells expressing ASC.

Increased amount of caspase-1 protein may be regulated at the level of mRNA (transcription and post-transcription) or protein (protein stability and translation). We showed that DHA accelerated caspase-1 protein synthesis. Interestingly, we perceived that increased caspase-1 protein synthesis concurred with suppressed GAPDH and ERK2 protein synthesis upon DHA treatment, suggesting that DHA specifically augments caspase-1 protein synthesis while shutting down others. Cellular stresses including oxidative stress have been shown to turn on the translational machinery of specific genes while suppressing the global protein translation.[28,37] Our observations that DHA elevated cellular level of ROS and NAC constrained DHA-induced caspase-1 upregulation in ovarian cancer cells suggest that DHA induces severe oxidative stress, which specifically augments caspase-1 protein synthesis and induces pyroptosis. ROS can activate Akt,[38,39] Erk,[39,40] and $p38^{MAPK}$,[41] 3 major signaling pathways involved in protein translation.[42–44] Surprisingly, we found that DHA only activated the $p38^{MAPK}$-Mnk1 signaling pathway. ROS is a common name for diverse chemical species.[37] Sole activation of $p38^{MAPK}$ signaling pathway by DHA implicates that a particular ROS may only activate certain signaling pathway(s) and ROS generated by DHA is specific for the activation of $p38^{MAPK}$. Collectively, we conclude that DHA-led oxidative stress activates the $p38^{MAPK}$-Mnk1 signaling pathway, leading to a specific translational augmentation of caspase-1 protein and subsequent pyroptosis in ovarian cancer cells.

Preclinical effects of DHA have been investigated in various cancer types. With limited number of nude mice, we showed that DHA was able to suppress intraperitoneal xenograft development. Although our *in vivo* study needs to be further expanded to confirm our findings, we did detect elevated caspase-1 staining in tumor implants recovered from mice receiving DHA and thus indicating the occurrence of pyroptosis in DHA-treated tumors. Our observation that DHA induces pyroptosis in ovarian cancer cells holds a particular promise to ovarian cancer immunotherapy given the fact that ovarian cancer, especially HGSOC, is generally unresponsive to immunotherapy.[45] Occurrence of

pyroptosis in ovarian cancer is expected to release cellular antigens, damage-associated molecular patterns (DAMPs), and cytokines, which are all capable of reversing immunosuppression of the tumor microenvironment and enhance tumor antigen presentation by dendritic cells.[46] A recent study showed that induction of pyroptosis by nanoparticle-delivered active GSDMD greatly sensitized mammary tumors to anti-PD1 therapy.[47] More significantly, pyroptosis of less than 15% of tumor cells was revealed to be sufficient to clear entire tumor grafts by anti-PD1 therapy.[47] Another study showed that initiating GSDMB-dependent pyroptosis of tumor cells led to robust cytotoxic lymphocyte-mediated cell killing, turning a "cold" tumor to a "hot" one.[48] Therefore, we reckon that, while DHA triggers pyroptosis in ovarian cancer cells, the event of pyroptosis can also simultaneously convert non-immunogenic ovarian cancer to immunogenic one. In future study, we will investigate the effect of DHA or other unsaturated fatty acids on antitumor immunity in ovarian cancer models including patient-derived organoids and immunocompetent mouse. Especially, we will determine the potential of using DHA to boost anti-PD1 and anti-PD-L1 therapies in ovarian cancer models.

In summary, our study has uncovered a previously unknown pyroptosis mechanism that is caspase-1-dependent but ASC/inflammasome-independent. Moreover, our experimental evidences demonstrate that this novel pyroptosis mechanism relies on the augmentation of caspase-1 protein translation.

Limitations of the study

DHA induces apoptosis in various cancer cell types including lung and colon cancer. However, we found that DHA triggered caspase-1-dependent pyroptosis in ovarian cancer cells. It is currently unclear whether DHA can also kill cells through pyroptosis besides ovarian cancer cells. We also showed that DHA accelerates caspase-1 protein synthesis in ovarian cancer cells via the $p38^{MAPK}$/Mnk1 signaling pathway, but exact sequence motifs in caspase-1 mRNA and involved factors for this process awaits to be identified. In future studies, we hope to address aforementioned aspects, and thus identify ways to specifically/effectively kills ovarian cancer cells.

STAR★METHODS

Detailed methods are provided in the online version of this paper and include the following:

- KEY RESOURCES TABLE
- RESOURCE AVAILABILITY
  - Lead contact
  - Materials availability
  - Data and code availability
- EXPERIMENTAL MODEL AND STUDY PARTICIPANT DETAILS
  - Cell culture
  - Mouse xenograft models, imaging, and drug administration
- METHOD DETAILS
  - Cell viability assay and IC50 determination
  - Cell cycle analysis
  - Inhibitor treatments
  - Caspase-1 activity assay, IL-1β ELISA, and LDH release assay
  - RNA isolation and RT-qPCR
  - Protein stability assay
  - Protein translation assay
  - Western blot analysis
  - Immunofluorescence staining
  - Lentivirus packaging and caspase-1 transfection
  - Reactive oxygen species (ROS) analysis
- QUANTIFICATION AND STATISTICAL ANALYSIS

SUPPLEMENTAL INFORMATION

Supplemental information can be found online at https://doi.org/10.1016/j.isci.2023.108408.

ACKNOWLEDGMENTS

This is part of the doctoral work of Ozlem Calbay at the University of Florida College of Medicine. This work was supported by funding from NIH CA222467 (SH) and CA256482 (SH/LJ).

AUTHOR CONTRIBUTIONS

O.C., R.P., M.A., L.S., B.L., N.Q., and J.G. performed research and analyzed results; Z.F. and L.J. provided experimental assistance and discussed results; O.C. and S.H. designed research and wrote the manuscript.

DECLARATION OF INTERESTS

The authors declare no competing interests.

INCLUSION AND DIVERSITY

We support inclusive, diverse, and equitable conduct of research.

Received: December 22, 2022
Revised: June 24, 2023
Accepted: November 3, 2023
Published: November 7, 2023

REFERENCES

1. Chen, X., He, W.T., Hu, L., Li, J., Fang, Y., Wang, X., Xu, X., Wang, Z., Huang, K., and Han, J. (2016). Pyroptosis is driven by non-selective gasdermin-D pore and its morphology is different from MLKL channel-mediated necroptosis. Cell Res. *26*, 1007–1020.
2. Matikainen, S., Nyman, T.A., and Cypryk, W. (2020). Function and Regulation of Noncanonical Caspase-4/5/11 Inflammasome. J. Immunol. *204*, 3063–3069.
3. Martinon, F., Burns, K., and Tschopp, J. (2002). The inflammasome: a molecular platform triggering activation of inflammatory caspases and processing of proIL-beta. Mol. Cell *10*, 417–426.
4. Broz, P., and Dixit, V.M. (2016). Inflammasomes: mechanism of assembly, regulation and signalling. Nat. Rev. Immunol. *16*, 407–420.
5. Shi, J., Zhao, Y., Wang, Y., Gao, W., Ding, J., Li, P., Hu, L., and Shao, F. (2014). Inflammatory caspases are innate immune receptors for intracellular LPS. Nature *514*, 187–192.
6. Peeters, P.M., Perkins, T.N., Wouters, E.F.M., Mossman, B.T., and Reynaert, N.L. (2013). Silica induces NLRP3 inflammasome activation in human lung epithelial cells. Part. Fibre Toxicol. *10*, 3.
7. Anderson, O.A., Finkelstein, A., and Shima, D.T. (2013). A2E induces IL-1ss production in retinal pigment epithelial cells via the NLRP3 inflammasome. PLoS One *8*, e67263.
8. Wang, H., Wang, Y., Du, Q., Lu, P., Fan, H., Lu, J., and Hu, R. (2016). Inflammasome-independent NLRP3 is required for epithelial-mesenchymal transition in colon cancer cells. Exp. Cell Res. *342*, 184–192.
9. Sun, P., Zhong, J., Liao, H., Loughran, P., Mulla, J., Fu, G., Tang, D., Fan, J., Billiar, T.R., Gao, W., and Scott, M.J. (2022). Hepatocytes Are Resistant to Cell Death From Canonical and Non-Canonical Inflammasome-Activated Pyroptosis. Cell. Mol. Gastroenterol. Hepatol. *13*, 739–757.
10. D'Eliseo, D., and Velotti, F. (2016). Omega-3 Fatty Acids and Cancer Cell Cytotoxicity: Implications for Multi-Targeted Cancer Therapy. J. Clin. Med. *5*, 15.
11. Tsai, W.S., Nagawa, H., Kaizaki, S., Tsuruo, T., and Muto, T. (1998). Inhibitory effects of n-3 polyunsaturated fatty acids on sigmoid colon cancer transformants. J. Gastroenterol. *33*, 206–212.
12. Fukui, M., Kang, K.S., Okada, K., and Zhu, B.T. (2013). EPA, an omega-3 fatty acid, induces apoptosis in human pancreatic cancer cells: role of ROS accumulation, caspase-8 activation, and autophagy induction. J. Cell. Biochem. *114*, 192–203.
13. Chamras, H., Ardashian, A., Heber, D., and Glaspy, J.A. (2002). Fatty acid modulation of MCF-7 human breast cancer cell proliferation, apoptosis and differentiation. J. Nutr. Biochem. *13*, 711–716.
14. Hu, Y., Sun, H., Owens, R.T., Gu, Z., Wu, J., Chen, Y.Q., O'Flaherty, J.T., and Edwards, I.J. (2010). Syndecan-1-dependent suppression of PDK1/Akt/bad signaling by docosahexaenoic acid induces apoptosis in prostate cancer. Neoplasia *12*, 826–836.
15. Pizato, N., Luzete, B.C., Kiffer, L.F.M.V., Corrêa, L.H., de Oliveira Santos, I., Assumpção, J.A.F., Ito, M.K., and Magalhães, K.G. (2018). Omega-3 docosahexaenoic acid induces pyroptosis cell death in triple-negative breast cancer cells. Sci. Rep. *8*, 1952.
16. Perez, M.A., Magtanong, L., Dixon, S.J., and Watts, J.L. (2020). Dietary Lipids Induce Ferroptosis in Caenorhabditiselegans and Human Cancer Cells. Dev. Cell *54*, 447–454.e4.
17. West, L., Yin, Y., Pierce, S.R., Fang, Z., Fan, Y., Sun, W., Tucker, K., Staley, A., Zhou, C., and Bae-Jump, V. (2020). Docosahexaenoic acid (DHA), an omega-3 fatty acid, inhibits tumor growth and metastatic potential of ovarian cancer. Am. J. Cancer Res. *10*, 4450–4463.
18. Bilyk, O., Hamedi, B., Dutta, I., Newell, M., Bukhari, A.B., Gamper, A.M., McVea, R.C., Liu, J., Schueler, J., Siegers, G.M., et al. (2022). Docosahexaenoic Acid in the Inhibition of Tumor Cell Growth in Preclinical Models of Ovarian Cancer. Nutr. Cancer *74*, 1431–1445.
19. Song, E.A., and Kim, H. (2016). Docosahexaenoic Acid Induces Oxidative DNA Damage and Apoptosis, and Enhances the Chemosensitivity of Cancer Cells. Int. J. Mol. Sci. *17*, 1257.
20. Bergsbaken, T., and Cookson, B.T. (2007). Macrophage activation redirects yersinia-infected host cell death from apoptosis to caspase-1-dependent pyroptosis. PLoS Pathog. *3*, e161.
21. Krumschnabel, G., Ebner, H.L., Hess, M.W., and Villunger, A. (2010). Apoptosis and necroptosis are induced in rainbow trout cell lines exposed to cadmium. Aquat. Toxicol. *99*, 73–85.
22. Miao, E.A., Rajan, J.V., and Aderem, A. (2011). Caspase-1-induced pyroptotic cell death. Immunol. Rev. *243*, 206–214.
23. Hu, J.J., Liu, X., Xia, S., Zhang, Z., Zhang, Y., Zhao, J., Ruan, J., Luo, X., Lou, X., Bai, Y., et al. (2020). FDA-approved disulfiram inhibits pyroptosis by blocking gasdermin D pore formation. Nat. Immunol. *21*, 736–745.
24. Compan, V., Martín-Sánchez, F., Baroja-Mazo, A., López-Castejón, G., Gomez, A.I., Verkhratsky, A., Brough, D., and Pelegrín, P. (2015). Apoptosis-associated speck-like protein containing a CARD forms specks but does not activate caspase-1 in the absence of NLRP3 during macrophage swelling. J. Immunol. *194*, 1261–1273.
25. Balakrishnan, A., Karki, R., Berwin, B., Yamamoto, M., and Kanneganti, T.D. (2018). Guanylate binding proteins facilitate caspase-11-dependent pyroptosis in response to type 3 secretion system-negative Pseudomonas aeruginosa. Cell Death Dis. *4*, 3.
26. Greenbaum, D., Colangelo, C., Williams, K., and Gerstein, M. (2003). Comparing protein abundance and mRNA expression levels on a genomic scale. Genome Biol. *4*, 117.
27. Belda-Palazón, B., Ferrando, A., and Farràs, R. (2016). Quantitation of Protein Translation Rate In Vivo with Bioorthogonal Click-Chemistry. Methods Mol. Biol. *1449*, 369–382.
28. Liu, B., and Qian, S.B. (2014). Translational reprogramming in cellular stress response. Wiley Interdiscip Rev RNA *5*, 301–315.
29. Pettersen, K., Monsen, V.T., Hakvåg Pettersen, C.H., Overland, H.B., Pettersen, G., Samdal, H., Tesfahun, A.N., Lundemo, A.G., Bjørkøy, G., and Schønberg, S.A. (2016). DHA-induced stress response in human colon cancer cells - Focus on oxidative stress and autophagy. Free Radic. Biol. Med. *90*, 158–172.
30. Tanaka, A., Yamamoto, A., Murota, K., Tsujiuchi, T., Iwamori, M., and Fukushima, N. (2017). Polyunsaturated fatty acids induce ovarian cancer cell death through ROS-dependent MAP kinase activation. Biochem. Biophys. Res. Commun. *493*, 468–473.
31. Ramalingam, S., Ramamurthy, V.P., Gediya, L.K., Murigi, F.N., Purushottamachar, P., Huang, W., Choi, E.Y., Zhang, Y., Vasaitis, T.S., Kane, M.A., et al. (2019). The Novel Mnk1/2 Degrader and Apoptosis Inducer VNLG-152 Potently Inhibits TNBC Tumor Growth and Metastasis. Cancers *11*, 299.
32. Sagulenko, V., Thygesen, S.J., Sester, D.P., Idris, A., Cridland, J.A., Vajjhala, P.R., Roberts, T.L., Schroder, K., Vince, J.E., Hill, J.M., et al. (2013). AIM2 and NLRP3 inflammasomes activate both apoptotic and pyroptotic death pathways via ASC. Cell Death Differ. *20*, 1149–1160.
33. Jing, W., Pilato, J.L., Kay, C., Feng, S., Tuipulotu, D.E., Mathur, A., Shen, C., Ngo, C., Zhao, A., Miosge, L.A., et al. (2022). Clostridium septicum alpha-toxin activates the NLRP3 inflammasome by engaging GPI-anchored proteins. Sci. Immunol. *7*, eabm1803.

34. Williams-Bey, Y., Boularan, C., Vural, A., Huang, N.N., Hwang, I.Y., Shan-Shi, C., and Kehrl, J.H. (2014). Omega-3 free fatty acids suppress macrophage inflammasome activation by inhibiting NF-kappaB activation and enhancing autophagy. PLoS One *9*, e97957.
35. Yan, Y., Jiang, W., Spinetti, T., Tardivel, A., Castillo, R., Bourquin, C., Guarda, G., Tian, Z., Tschopp, J., and Zhou, R. (2013). Omega-3 fatty acids prevent inflammation and metabolic disorder through inhibition of NLRP3 inflammasome activation. Immunity *38*, 1154–1163.
36. Van Opdenbosch, N., Gurung, P., Vande Walle, L., Fossoul, A., Kanneganti, T.D., and Lamkanfi, M. (2014). Activation of the NLRP1b inflammasome independently of ASC-mediated caspase-1 autoproteolysis and speck formation. Nat. Commun. *5*, 3209.
37. Ghosh, A., and Shcherbik, N. (2020). Effects of Oxidative Stress on Protein Translation: Implications for Cardiovascular Diseases. Int. J. Mol. Sci. *21*, 2661.
38. Kim, J.H., Na, H.J., Kim, C.K., Kim, J.Y., Ha, K.S., Lee, H., Chung, H.T., Kwon, H.J., Kwon, Y.G., and Kim, Y.M. (2008). The non-provitamin A carotenoid, lutein, inhibits NF-kappaB-dependent gene expression through redox-based regulation of the phosphatidylinositol 3-kinase/PTEN/Akt and NF-kappaB-inducing kinase pathways: role of H(2)O(2) in NF-kappaB activation. Free Radic. Biol. Med. *45*, 885–896.
39. Li, Q., Fu, G.B., Zheng, J.T., He, J., Niu, X.B., Chen, Q.D., Yin, Y., Qian, X., Xu, Q., Wang, M., et al. (2013). NADPH oxidase subunit p22(phox)-mediated reactive oxygen species contribute to angiogenesis and tumor growth through AKT and ERK1/2 signaling pathways in prostate cancer. Biochim. Biophys. Acta *1833*, 3375–3385.
40. Preston, T.J., Muller, W.J., and Singh, G. (2001). Scavenging of extracellular H2O2 by catalase inhibits the proliferation of HER-2/Neu-transformed rat-1 fibroblasts through the induction of a stress response. J. Biol. Chem. *276*, 9558–9564.
41. Liu, Y., Shi, Q.F., Ye, Y.C., Tashiro, S.i., Onodera, S., and Ikejima, T. (2012). Activated O2(*-) and H2O2 mediated cell survival in SU11274-treated non-small-cell lung cancer A549 cells via c-Met-PI3K-Akt and c-Met-Grb2/SOS-Ras-p38 pathways. J. Pharmacol. Sci. *119*, 150–159.
42. Mamane, Y., Petroulakis, E., Rong, L., Yoshida, K., Ler, L.W., and Sonenberg, N. (2004). eIF4E–from translation to transformation. Oncogene *23*, 3172–3179.
43. Raught, B., and Gingras, A.C. (1999). eIF4E activity is regulated at multiple levels. Int. J. Biochem. Cell Biol. *31*, 43–57.
44. Wang, X., Flynn, A., Waskiewicz, A.J., Webb, B.L., Vries, R.G., Baines, I.A., Cooper, J.A., and Proud, C.G. (1998). The phosphorylation of eukaryotic initiation factor eIF4E in response to phorbol esters, cell stresses, and cytokines is mediated by distinct MAP kinase pathways. J. Biol. Chem. *273*, 9373–9377.
45. Wan, C., Keany, M.P., Dong, H., Al-Alem, L.F., Pandya, U.M., Lazo, S., Boehnke, K., Lynch, K.N., Xu, R., Zarrella, D.T., et al. (2021). Enhanced Efficacy of Simultaneous PD-1 and PD-L1 Immune Checkpoint Blockade in High-Grade Serous Ovarian Cancer. Cancer Res. *81*, 158–173.
46. Fang, Y., Tang, Y., and Huang, B. (2023). Pyroptosis: A road to next-generation cancer immunotherapy. Semin. Immunol. *68*, 101782.
47. Wang, Q., Wang, Y., Ding, J., Wang, C., Zhou, X., Gao, W., Huang, H., Shao, F., and Liu, Z. (2020). A bioorthogonal system reveals antitumour immune function of pyroptosis. Nature *579*, 421–426.
48. Zhou, Z., He, H., Wang, K., Shi, X., Wang, Y., Su, Y., Wang, Y., Li, D., Liu, W., Zhang, Y., et al. (2020). Granzyme A from cytotoxic lymphocytes cleaves GSDMB to trigger pyroptosis in target cells. Science *368*, eaaz7548.
49. Elegheert, J., Behiels, E., Bishop, B., Scott, S., Woolley, R.E., Griffiths, S.C., Byrne, E.F.X., Chang, V.T., Stuart, D.I., Jones, E.Y., et al. (2018). Lentiviral transduction of mammalian cells for fast, scalable and high-level production of soluble and membrane proteins. Nat. Protoc. *13*, 2991–3017.

STAR★METHODS

KEY RESOURCES TABLE

REAGENT or RESOURCE	SOURCE	IDENTIFIER
Antibodies		
Akt Rabbit polyclonal	Cell Signaling	#9272
ASC (clone 2EI-7) Mouse monoclonal	EMD, Sigma-Aldrich	#04-147
Caspase1 Rabbit polyclonal	Proteintech	#22915-1-AP
Caspase3 Rabbit polyclonal	Cell Signaling	#9662
eIF4E Rabbit polyclonal	Cell Signaling	#9742S
GAPDH Rabbit monoclonal	Cell Signaling	#2118
GSDMD Mouse monoclonal	Proteintech	#66387-1-Ig
Mnk1 (C4C1) Mouse monoclonal	Cell Signaling	#2195S
p38 MAPK Rabbit polyclonal	Cell Signaling	#9212S
p44/42 MAPK (Erk1/2) Rabbit polyclonal	Cell Signaling	#9102S
PARP (46D11) Rabbit monoclonal	Cell Signaling	#9532
Phospho-Akt (Ser473) (D9E) Rabbit monoclonal	Cell Signaling	#4060S
Phospho-eIF4E (Ser209) Rabbit polyclonal	Cell Signaling	#9741S
Phospho-Mnk1 (Thr197/202) Rabbit polyclonal	Cell Signaling	#2111
Phospho-p44/42 MAPK (Erk1/2) (Thr202/Thr204) Rabbit polyclonal	Cell Signaling	#9101S
Phospho–p38 (Thr180/Thr182) (D3F9) Rabbit monoclonal	Cell Signaling	#4511S
Chemicals, peptides, and recombinant proteins		
Adenosine 5′-triphosphate (ATP)	Sigma-Aldrich	#A2383
Click-IT™ AHA (L-Azidohomoalanine)	Invitrogen™	#C10102
AZD5363	Selleckchem	#S8019
Biotin-PEG4-alkyne	Sigma-Aldrich	#764213
BIRB796	Selleckchem	#S1574
Chloroquine	Sigma-Aldrich	#1118000
CPG57380	Selleckhem	#S7421
Complete™, Mini, EDTA-free Protease Inhibitor Cocktail	Roche	#11836170001
Click-iT™ Protein Reaction Buffer Kit	Invitrogen™	#C10276
Crystal violet solution 1%	Sigma-Aldrich	# 548-62-9
Cycloheximide (CHX)	Sigma-Aldrich	#C4859
CM-H2DCFDA (General Oxidative Stress Indicator)	Invitrogen™	#C6827
Disulfiram	Tocris	#3807
Dimethyl Sulfoxide (DMSO)	Fisher Scientific	#D1391
DNase I (RNase-free)	New England Biolabs	#M0303L
Fetal Bovine Serum, Tet system approved, USDA-approved regions	Gibco™	#A4736401
Filter (small) 10 µm pore size	MoBiTec GmbH	#M2110
Goat anti-Rabbit IgG (H + L) Cross-Adsorbed Secondary Antibody, Alexa Fluor™ 488	Invitrogen	#A-11008
Goat anti-Mouse IgG (H + L) Highly Cross-Adsorbed Secondary Antibody, Alexa Fluor™ 594	Invitrogen	#A-11032
Hoechst 33342 Solution (20 mM)	Thermo Scientific™	#62249

(*Continued on next page*)

Continued

REAGENT or RESOURCE	SOURCE	IDENTIFIER
IGEPAL® CA-630	Sigma-Aldrich	#9002-93-1
DMEM, high glucose, no glutamine, no methionine, no cystine	Gibco™	#21013024
MCC950	Selleckchem	#S7809
M-MLV Reverse Transcriptase (200 U/μL)	Invitrogen™	#28025013
MTT (3- [4,5-dimethylthiazol-2-yl]-2,5 diphenyl tetrazolium bromide)	Sigma-Aldrich	#M2128
N-acetyl cysteine (NAC)	Sigma-Aldrich	#A7250
Necrostatin	Tocris	#2324/10
Paraformaldehyde, 4% in PBS	Thermo Scientific	# AAJ61899AK
PD MiniTrap G-25	Cytiva	#28918007
Puromycine	Gibco	#A1113803
Pierce™ Bovine Serum Albumin Standard Ampules, 2 mg/mL	Thermo Scientific™	#23209
Pierce™ ECL Western Blotting Substrate	Thermo Scientific™	#32106
Pierce™ BCA Protein Assay Kit	Thermo Scientific™	#23225
Rapamycine	Selleckhem	#S1039
SDS-PAGE Protein Loading Buffer 5X (Reducing)	Boster	#SKU:AR1112
Streptavidin–Agarose from Streptomyces avidinii	Millipore	#S1638
Trametinib	Selleckchem	#S2673
Trizol	Thermo Fisher	#15596018
Triton™ X-100	Sigma-Aldrich	#X100
Z-DEVD-FMK	Selleckchem	#S7312
Z-YVAD-FMK	Selleckchem	#S8507
ProLong™ Glass Antifade Mountant	Invitrogen	#P36980
Critical commercial assays		
Propidium Iodide Flow Cytometry Kit	Abcam	#ab139418
Caspase-1/ICE Colorimetric Assay Kit	R&D system	#BF15100
Human IL-1 beta/IL-1F2 Quantikine ELISA Kit	R&D system	#DLB50
Pierce LDH Cytotoxicity Assay Kit	Thermo Scientific	#88953
Oligonucleotides		
Caspase1	forward GCTTTCTGCTCTTCCACACCA	reverse AAATGAAAATCGAACCTTGCGGA
BetaActin	forward CCAGCTCACCATGGATGATG	reverse ATGCCGGAGCCGTTGTC
Software and algorithms		
GraphPad Prism	Software	8
Flow Jo	Software	10.4
ImageJ	Software	National Institute of Health
NIS Element Viewer	Software	Nikon

RESOURCE AVAILABILITY

Lead contact

Further information and requests for resources and reagents should be directed to and will be fulfilled by the lead contact author, Shuang Huang (shuanghuang@ufl.edu).

Materials availability

This study did not generate new unique reagents.

Data and code availability

- This paper did not generate any omics dataset. All data reported in this paper will be shared by the lead contact upon request.
- This paper does not report original code.
- Any additional information required to reanalyze the data reported in this paper is available from the lead contact upon request.

EXPERIMENTAL MODEL AND STUDY PARTICIPANT DETAILS

Cell culture

Nine established human ovarian cancer cell lines were used in this study. They are CaOV3, ES2, HEY, IGROV1, OCC1, OVCAR3, OVCAR4, OVCAR5 and SK-OV3. CaOV3, ES2, HEY, OVCAR3 and SK-OV3 were purchased from American Tissue Culture Collection (Manassas, VA). IGROV1 was obtained from MilliporeSigma (Burlington, MA). OCC1, OVCAR4 and OVCAR5 were provided by Dr. Yan Xu (Indiana University). All cell lines were cultured in Dulbecco's modified Eagle's medium supplemented with 10% FBS (Gibco, Cat#A4736401) under humidified conditions at 37°C and 5% CO_2. The authenticities of these cell lines are verified once a year by the JH-Nucleic Acid Technologies, Johns Hopkins University (Baltimore, MD) using PowerPex 180 Kit.

Mouse xenograft models, imaging, and drug administration

ES2 cells containing luciferase gene were intraperitoneally injected into 5–6-week-old nude female mice (1×10^6 cells/mouse) (Jackson Lab, Bar Harbor, ME) and intraperitoneal xenograft development was monitored weekly by measuring fluorescence in Xenogen IVIS-200 *In Vivo* Bioluminescence imaging system (PerkinElmer Inc, Waltham, MA). After 1 week of tumor cell injection, mice were randomized into two groups (5 per group) and intraperitoneally injected with vehicle (DMSO) or DHA daily (15mg/Kg). At week 5, mice were sacrificed, and visible implants were collected from peritoneal cavities. Collected implants were weighed and aliquot of implants were also sent to UF Pathology core for immunohistochemistry staining of caspase-1, cleaved caspase-3 and Ki67. Animal studies and these procedures were approved by the Institution Animal Care Committee at University of Florida.

METHOD DETAILS

Cell viability assay and IC50 determination

Cells were seeded overnight at a density of 10,000 cells per well in 24-well plates and then exposed to varying concentrations of DHA for 24 or 48 hours. Cell viability was assessed by adding MTT (Sigma, Cat # M2128) to the cells followed by incubation at 37°C for 1 hour. The MTT formazan crystals generated were dissolved in DMSO, and optical density was measured at 570 nm using a Bio-Rad plate reader. The IC_{50} value of DHA was determined by GraphPad software 8.0 (San Diego, USA).

Cell cycle analysis

ES2, SKOV3, and OCC1 cells (1.5×10^5cells/well) were seeded in 6-well plates overnight and exposed to DHA (0, 60, 100 μM) at 37°C for 24 or 48 hours. After several washes, cells were detached, fixed in cold ethanol, and stained with propidium iodide (PI) in accordance with the manufacturer's guidelines (Abcam, Cat #ab139418). Cell cycle analysis was performed using a flow cytometer (BD Accuri C6 Plus) and analyzed by Flow Jo software.

Inhibitor treatments

To investigate the mechanism underlying DHA-induced cell death, cells were seeded overnight at a density of 10,000 cells per well in 24-well plates. Cells were next pretreated with 20 μM of Z-DEVD-FMK, 20 μM of Z-YVAD-FMK or 1 μM of necrostatin for 2 hours before incubation with DHA or vehicle for another 24 hours. Cell viability was assessed by MTT assay.

To examine the role of Gasdermin D in DHA-induced cell death, cells were seeded at a density of 1.5x105 cells per well in 6-well plates and treated with DHA in the absence or presence of 1 μM disulfiram for another 24 hours. Cells were fixed with 4% paraformaldehyde and stained with 0.1% crystal violet. Stained cells were visualized using phase-contrast microscopy (Carl Zeiss Vision, LSM510), and the crystal violet dye was quantified at 595 nm using a Bio-Rad plate reader.

To investigate the signaling pathways involved in DHA-induced cell death, cells cultured overnight (1.5×105 cells per well in 6-well plates) were pretreated with 10 μM Trametinib, 10 μM AZD5363, 10 μM CPG57380, or 10 μM BIRB796 for 2 hours prior to DHA treatment. Cell viability was evaluated using both MTT and crystal violet staining after 24 hours. The involvement of NLRP3 in pyroptosis was analyzed by seeding mouse macrophages (4×105 cells per well in 6-well plates) or ovarian cancer cells overnight, followed by treatment with respective 5 mM ATP or DHA with or without 5 μM MCC950 (30 min for ATP treatment in macrophages and 24 hours for DHA treatment in ovarian cancer cells). Cell viability was determined by crystal violet staining.

Caspase-1 activity assay, IL-1β ELISA, and LDH release assay

ES2, SKOV3 and OCC1 cells were seeded at a density of 1.5×10^5 cells per well in 6-well plate and treated with either DHA or vehicle for 24 hours. Cells were pelleted to measure caspase-1 activity using colorimetric caspase-1 activity assay kit (R&D system, Cat # BF15100), and cell

culture media were collected for detection of IL-1β using IL-1β ELISA detection kit (R&D system, Cat # DLB50) and LDH release using LDH activity kit (Thermo Fisher, Cat # 88953), according to the manufacturer's instructions.

RNA isolation and RT-qPCR

Total RNA was extracted using Trizol, then treated with DNase I and used for cDNA synthesis using M-MLV reverse transcriptase. The generated cDNA was subjected to qPCR to measure levels of Caspase-1 and β-Actin mRNA. The level of β-Actin was used as an internal control for standardization. The primer sequences for Caspase-1 mRNA are forward GCTTTCTGCTCTTCCACACCA and reverse AAATGAA AATCGAACCTTGCGGA. The primer sequences for β-Actin mRNA are forward CCAGCTCACCATGGATGATG and reverse ATGCCG GAGCCGTTGTC.

Protein stability assay

ES2, SKOV3 and OCC1 cells (1.5×10^5 cells per well in 6-well plates) were cultured overnight and then treated with DHA for 24 hours followed by adding 10μg/ml cycloheximide. At varying time, cells were lysed and cell lysates were subjected to western blot to detect caspase-1 and GAPDH using respective antibodies. The amount of caspase-1 or GAPDH protein was quantified by measuring the intensity of each band using Image J software.

Protein translation assay

We measure protein synthesis rate using a click chemistry-based protocol developed by Belda-Palazón et al.[27] ES2, SKOV3, and OCC1 cells (1.5×10^5 cells per well in 6-well plates) were grown in regular medium until sub-confluent, then starved for 1 hour with DMEM-Met medium (Gibco, Cat#21013024) at 37 °C. Cells were treated with vehicle or DHA in DMEM-Met medium containing 50 μM of methionine biorthogonal L-Azidohomoalanine (AHA) (Invitrogen, cat #C10102) and harvested at varying times (0, 2, 4, 8, and 16 h). After washing cells with cold PBS, cell pellets were stored at −80°C.

AHA-labeled proteins were extracted from cell pellets using Protein Extraction Buffer (PEB), and protein concentration was determined by BCA assay (Thermo Scientific™, Cat#23225). Subsequently, 200 μg of protein was incubated with click-IT reaction buffer (Invitrogen™, Cat#C10276) in the presence of biotin-PEG4 alkyne (Sigma-Aldrich, #764213) followed by removing excessive biotin-PEG4 alkyne using Minitrap G25 columns (Cytiva, Cat#28918007). Streptavidin-Agarose beads (Millipore, Cat#S1638) were added to elute and further subjected to affinity purification with 10 μm pore size filters (MoBiTec GmbH, Cat# M2110). The final elute was boiled in Laemmli buffer and further analyzed by western blot to detect caspase-1 and GAPDH using the respective antibodies (see the schematic diagram in Figure S9). This assay selectively pulls down AHA-containing proteins (newly synthesized proteins) and thus be used to assess protein synthesis rate.

Western blot analysis

Cells were lysed with RIPA buffer (50 mM Tris-Cl, pH 7.4, 150 mM NaCl, 1% Triton, 0.1% SDS, 0.5% Sodium deoxycholate, 2 mM EDTA and a cocktail of protease inhibitors). The amount of protein was measured using the BCA assay (Thermo Scientific™, Cat#23225) according to the manufacturer's instructions. Cell lysates were then boiled in protein loading buffer (Boster, Cat# SKU: AR1112) and separated on an 8-12% SDS–polyacrylamide gel. The separated proteins were transferred to nitrocellulose membranes using wet electronic transfer apparatus for 90 minutes. The membranes were blocked with 5% nonfat dry milk for 1 hour at room temperature and then probed with primary antibodies overnight. After several washes, the membranes were incubated with secondary antibody conjugated to horseradish peroxidase at a 1:20,000 dilution, developed using ECL (Thermo Scientific™ Cat#32106), and imaged on GE/Amersham Imager 680.

Immunofluorescence staining

Ovarian cancer cells were seeded on coverslips overnight and then treated with DHA or vehicle for 24 hours followed by fixation using 4% paraformaldehyde. Fixed cells were permeabilized with 1% Triton X-100, blocked with 1% BSA and incubated with anti-Casp1 polyclonal antibody (1:100 dilution) or anti-ASC mAb (1:200 dilution). Subsequently, coverslips were incubated with a secondary antibody (Alexa Fluor 488 goat anti-rabbit (Invitrogen, Cat#A-11008) or Alexa 594 goat anti-mouse antibody (Invitrogen, Cat#A-11032),) followed by mounting on glass slides using an Anti-Fade mount containing DAPI (Thermo Fisher). The slides were viewed using confocal microscopy (Nikon Eclipse Ti, N-Storm). For mouse macrophage cells, cells were seeded on coverslips overnight and then treated with 5mM ATP before immunofluorescence staining as described for ovarian cancer cells.

Lentivirus packaging and caspase-1 transfection

Lentiviral vector (pLKO.1) containing PYCARD (ASC) shRNA were obtained from Sigma-Aldrich TRC collection (TRCN0000059073 and TRCN0000059075) (Burlington, MA) and used to generate lentivirus according to a protocol developed by Elegheert et al.[49] To silence ASC, ES2, SK-OV3 and OCC1 cells were infected with the lentivirus for 2 days and subsequently selected with puromycin (2μg/ml) for an additional 2 days before conducting any further experiments.

Reactive oxygen species (ROS) analysis

Cells were treated with DHA for 1, 3, 6 and 12 h or H_2O_2 for 2 hours and detached by trypsinization. Detached cells were resuspended, in PBS containing 2μM CM-H2DCFDA (Cat # C6827, Thermo Fisher) for 15 min at 37 °C followed by flow cytometer (BD Accuri C6 Plus) at a 488 nm channel. For each sample, 10,000 cells were analyzed. Data analysis was performed using FlowJo 10.4 software.

QUANTIFICATION AND STATISTICAL ANALYSIS

Data are presented as the mean ± SEM of triplicate experiments. Statistical significance was calculated using one way ANOVA and student *t* test. $P < 0.05$ was considered statistically significant. All statistical analyses were conducted with the aid of GraphPad Prism 8.0 or Microsoft Excel.